Nonlinear harmonic balance modelling for wave energy converter array layout assessment

Trends in Renewable Energies Offshore – Guedes Soares (Ed)

Nonlinear harmonic balance modelling for wave energy converter array layout assessment

D. García-Violini
Universidad Nacional de Quilmes, Buenos Aires, Argentina
CONICET, Buenos Aires, Argentina

Y. Peña-Sánchez
Euskal Herriko Unibertsitatea (EHU/UPV), Leioa, Bizkaia, Spain

A. Zarketa
Fluid Mechanics Department, Mondragon University, Arrasate, Gipuzkoa, Spain

M. Penalba
Fluid Mechanics Department, Mondragon University, Arrasate, Gipuzkoa, Spain
Ikerbasque, Basque Foundation for Science, Bilbao, Bizkaia, Spain

N. Faedo
Marine Offshore Renewable Energy Lab., Politecnico di Torino, Torino, Italy

J.V. Ringwood
Centre for Ocean Energy Research, Maynooth University, Maynooth, County Kildare, Ireland

ABSTRACT: Wave energy converters (WECs) are most likely to be deployed in large arrays to reduce their cost of energy. However, the energy production of such arrays can be both positively and negatively affected by hydrodynamic interactions. Therefore, array layouts need to be carefully optimised. Such optimisation is usually carried out via hydrodynamic models that neglect more complex descriptions of WECs (e.g. nonlinear and non-ideal effects in the hydrodynamics and power take-off system) and the impact of advanced control. However, the articulation of these effects is crucial, since they can strongly impact on the array performance, questioning the conclusions drawn from simplistic linear assessments. This paper suggests the harmonic balance (HB) method to assess the behaviour of WEC arrays, which can efficiently articulate nonlinearities. Results from the HB approach are identical to the steady-state solution of a traditional (nonlinear) time-domain simulation, while highlighting the potential for a significant computational cost reduction.

1 INTRODUCTION

The technological maturity of floating offshore wind turbines (FOWTs) has significantly increased in the recent years, with several prototypes close to the commercial stage. Nowadays, the sector is taking off and the first semi-commercial projects have already been assigned early this year in Scotland: 15GW out of a total of 25GW offshore wind being assigned for FOWT . In addition, two more FOWT farms are expected to be announced in France and Norway, demonstrating the positive trend towards the commercialisation of FOWT technologies. The wave energy sector, although slower than FOWTs, is also reaching higher levels of maturity. Several wave energy converter (WEC) technologies are getting closer to the commercialisation stage and the first pilot WEC array has already been announced in Portugal. In any case, offshore renewable energy systems, including both FOWTs and WECs, have a crucial role in the decarbonisation of the energy sector. Yet, due to the relatively low power of isolated FOWTs (about 10 MW) and WECs (below 1 MW), their future lies on large multi-MW arrays. The behaviour of FOWTs and WECs in these arrays can vary significantly due to the aero-hydrodynamic interaction between the different devices and, thus, the array layout needs to be carefully designed. Apart from the aero/hydrodynamic interaction, other aspects, such as shared mooring lines or electrical cables, must be evaluated in order to optimise these farms.

DOI: 10.1201/9781003360773-42

In the case of WECs, most of the studies in the literature focus on layout optimisation focused on hydrodynamic interaction. In this sense, conventional frequency-domain (FD) approaches have been widely used in the literature. For example, (Babarit 2010) analyses the impact on the absorbed wave power of the separating distance between WEC arrays with two devices using a FD numerical model which takes into account wave interaction. The simplicity and low computational cost of the FD domain model allows for studying the impact of different aspects on WEC arrays. Borgarino (Borgarino et al. 2012) evaluates the influence of hydrodynamic interaction between bodies on the annual mean energy production of the WEC array by means of a FD model, where different sizes of WEC arrays are considered. The same numerical model is also used in (Penalba et al. 2017), where different WEC array configurations including different WEC and array sizes are analysed, concluding that the impact of inter-device hydrodynamic interaction in the array tends to saturate as the size increases. Similarly, (Penalba et al. 2020) analysed the impact of long-term resource trends on the power generation capacity of WEC arrays of different sizes. Finally, an alternative approach in time-domain (TD) is suggested in (Gaebele et al. 2020), where a state-space model for WEC arrays that includes the PTO mechanism is presented.

However, the WEC hydrodynamic model, and controller descriptions, in these studies are too simplistic for drawing definitive conclusions. In this sense, (Garcia-Rosa et al. 2015) also analyses the layout optimisation for small arrays, but includes an advanced control strategy for energy maximisation, while non-ideal effects in the WEC model are ignored. Considering nonlinear and non-ideal effects, and the impact of the controller, is crucial for a precise assessment of WEC array layout. Yet, incorporating nonlinear and non-ideal effects is infeasible with traditional FD approaches, and computationally prohibitive by using TD methods. In this sense, the recent study presented in (Magana et al. 2021) suggests a nonlinear Model Predictive Control algorithm for the maximisation of the energy absorbed from WEC arrays, where nonlinerities of the oscillating water column chamber, due to air compressibility and PTO dynamics, are included. However, hydrodynamic nonlinearities are still neglected in this study and cannot be captured by the state-space model suggested by the authors. Therefore, the accurate analysis of WEC arrays requires a computationally inexpensive but precise modelling technique that enables efficient articulation of nonlinear and non-ideal effects.

In this context, the Harmonic Balance (HB) method seems an ideal choice, since it allows for the articulation of nonlinear effects, but with low computational burden by means of the hybrid frequency-time-domain approach. This approach has already been suggested in the literature for WEC modelling (Mérigaud and Ringwood 2017, Giorgi and Faedo 2022), articulating nonlinear hydrodynamic effects, and advanced controllers. In fact, the HB approach is also suggested for the analysis of WEC arrays (Wei et al. 2021), although nonlinear effects are restricted to the power take-off (PTO) system.

The present paper also suggests the HB approach for the assessment of WEC array layouts, but includes nonlinear hydrodynamic effects as a distinguishing factor compared to other studies in the literature. The model presented here serves as the basis for future articulation of other nonlinear hydrodynamic effects (*e.g.* nonlinear Froude-Krylov effects), nonlinear and non-ideal PTO effects, and advanced controllers.

The paper is organised as follows. Section 2 describes the mathematical model for WEC arrays, including hydrodynamic interaction effects; Section 3 defines the theoretical framework for the HB approach; Section 4 describes the case study analysed in this study; Section 5 presents and discusses the main results; and Section 6 draws the fundamental conclusions of the study and suggests the main development lines for future implementations of the HB approach.

2 WEC ARRAY SYSTEM

In this section, the basics behind WEC array modelling are introduced. For the sake of simplicity, the devices comprising the array are assumed to be geometrically identical and move in a single degree-of-freedom (DoF).

2.1 *WEC motion in the array*

Based on Newton's second law, a WEC array composed of n_b devices can be numerically described as follows,

$$\mathbf{m}\ddot{z}(t) = \sum_{i}^{N} f_i(t), \tag{1}$$

where $\mathbf{m} = m \cdot \mathbb{I}_{n_\mathrm{b}} \in \mathbb{R}^{n_\mathrm{b} \times n_\mathrm{b}}$, m being the mass of a considered isolated WEC, $\mathbb{I}_{n_\mathrm{b}} \in \mathbb{R}^{n_\mathrm{b} \times n_\mathrm{b}}$ the identity matrix, $f(t) \in \mathbb{R}^{n_\mathrm{b} \times 1}$ a vector with N different forces acting on the N devices of the array, and $z(t), \dot{z}(t)$, and $\ddot{z}(t) \in \mathbb{R}^{n_\mathrm{b} \times 1}$ the displacement, velocity, and acceleration of the WECs, respectively. In this study, without loss of generality, five different forces are considered, namely the hydrodynamic excitation force (f_ex), radiation force (f_r), hydrostatic restoring force (f_h), PTO force (f_pto), and viscous force (f_v). All these forces are considered as linear forces, except for the viscous force, which is represented as a quadratic function.

The excitation force refers to the force that the incoming waves exert on the devices. The restoring force is defined as $f_\mathrm{h} = \mathbf{k}_\mathrm{h} z(t)$, with $\mathbf{k}_\mathrm{h} = k_\mathrm{h} \cdot \mathbb{I}_{n_\mathrm{b}} \in \mathbb{R}^{n_\mathrm{b} \times n_\mathrm{b}}$ being a matrix containing the information of the hydrostatic stiffness (k_h) of all the devices in the array. The radiation force is given as described in Cummins' equation (Cummins 1962),

$$f_r(t) = \mathbf{h}_r \star \dot{z}(t) + \boldsymbol{\mu}\ddot{z}(t), \tag{2}$$

where the symbol $\star$ denotes convolution, and $\mathbf{h}_\mathrm{r} \in \mathbb{R}^{n_\mathrm{b} \times n_\mathrm{b}}$ and $\boldsymbol{\mu} \in \mathbb{R}^{n_\mathrm{b} \times n_\mathrm{b}}$ correspond to the radiation impulse response kernel and infinite frequency added mass ($\boldsymbol{\mu} = \lim_{\omega \to \infty} \mathbf{A}_\mathrm{r}(\omega)$) of each body (diagonal terms) and the interaction between devices (off-diagonal terms), respectively. The radiation kernel $\mathbf{h}_\mathrm{r}$ can be computed from the so-called radiation added-mass and damping coefficients ($\mathbf{A}_\mathrm{r}(\omega)$ and $\mathbf{B}_\mathrm{r}(\omega)$, respectively) following Ogilvie's relations (Ogilvie 1964). Note that inter-device hydrodynamic interaction is included in the radiation and excitation hydrodynamic coefficients, as illustrated in (Penalba et al. 2017).

For this analysis, the PTO force is computed as follows,

$$f_\mathrm{pto} = \mathbf{h}_\mathrm{pto}\dot{z} + \mathbf{k}_\mathrm{pto} z, \tag{3}$$

where $\mathbf{h}_\mathrm{pto} = h_\mathrm{pto}\mathbb{I}_{n_\mathrm{b}}$ and $\mathbf{k}_\mathrm{pto}k_\mathrm{pto}\mathbb{I}_{n_\mathrm{b}}$, with h_pto and k_pto the PTO damping and stiffness coefficients, respectively. Finally, the nonlinear viscous force is defined following the well-known Morison's equation (Morison et al. 1950) as,

$$f_\mathrm{v} = \mathbf{h}_\mathrm{d}\dot{z}(t)|\dot{z}(t)| \tag{4}$$

where $\mathbf{h}_d = h_\mathrm{d} \cdot \mathbb{I}_{n_\mathrm{b}} \in \mathbb{R}^{n_\mathrm{b} \times n_\mathrm{b}}$ and h_d is the viscous drag coefficient. Thus, Equation (1) can be re-written as,

$$\begin{aligned}\mathbf{M}\ddot{z}(t) \quad &= f_\mathrm{ex}(t) - (\mathbf{k}_\mathrm{h} + \mathbf{k}_\mathrm{pto})z(t) - \mathbf{h}_r \star \dot{z}(t) \\ &\quad -\mathbf{h}_\mathrm{pto}\dot{z}(t) - \mathbf{h}_\mathrm{d}\dot{z}(t)|\dot{z}(t)|,\end{aligned} \tag{5}$$

where $\mathbf{M} = \mathbf{m} + \boldsymbol{\mu}$.

Finally, it should be noted that additional forces in the WEC array description could be considered without loss of generality of the proposed HB strategy and negligible impact on the computational cost.

2.2 *WEC array power absorption*

Finally, the power production of the WEC array can be computed based on the motion of the devices in the array. Absorbed power is defined as the mechanical power absorbed by the WEC from ocean waves, where further conversion into other forms of mechanical energy (*i.e.* pneumatic energy in oscillating water column devices or hydraulic energy in hydraulic PTO systems) and electricity is neglected. Hence, the time-average power absorbed by the WEC array is given as follows:

$$P_{av} = \int_0^{t_{sim}} f_\mathrm{pto} \cdot \dot{z}(t)dt. \tag{6}$$

The impact of the inter-array hydrodynamic interaction on device behaviour can be analysed by comparing the body motion of a WEC in the array with an isolated WEC. However, comparison of the power absorption is not as straightforward, since the power absorption of each device in the array is not necessarily the same. Therefore, in the case of WEC arrays, a gain-factor or q-factor is usually employed, which allows for the study of absorbed power variations in percentage terms. The q-factor is defined between the power absorbed by an isolated device ($P_{isolated}$), the number of WECs in the array and the power absorbed by the complete array (P_{array}) as follows:

$$q = \frac{P_{array}}{N \cdot P_{isolated}}. \tag{7}$$

This q-factor can take any value, with $q = 1$ meaning that the hydrodynamic interaction is neutral, $q > 1$ meaning that interaction is constructive and $q < 1$ destructive. Constructive interaction means that the WECs in the array are able to absorb more energy than when isolated, due to the hydrodynamic interaction. In contrast, destructive interaction appears when the hydrodynamic interaction hampers the motion of the WECs in the arrays, resulting in lower power absorption compared to an isolated WEC.

3 HARMONIC BALANCE APPROACH

This section briefly describes the HB implementation considered in this study, which is based on the theory presented in (Giorgi and Faedo 2022). Harmonic balance is a well-known approach used to analyse the dynamics of nonlinear systems using an approximate harmonic representation of the corresponding system variables (Krack and Gross 2019).

Note that Equation (5) can be re-written in terms of a continuous-time state-space system as

$$\dot{x}(t) = f(x(t),\, f_\mathrm{ex}(t)), \tag{8}$$

where $x(t) = [\mathbf{z}(t)^\mathrm{T}\dot{\mathbf{z}}(t)(t)^\mathrm{T}]^\mathrm{T} \in \mathbb{R}^{2n_\mathrm{b} \times 1}$, and $\mathbf{z}(t)$ defined as in Equation (5) with f being the corresponding state-transition map, which can be derived from Equation (5). The excitation force $f_\mathrm{ex}(t)$ can be assumed to be described based on harmonic functions as follows:

$$f_\mathrm{ex}(t) = F_\mathrm{ex}\cos(\omega t), \tag{9}$$

where $F_\mathrm{ex} \in \mathbb{R}^+$ is the amplitude of the excitation force signal and ω the associated fundamental frequency. From now on, $T = 2\pi/\omega$ is referred to as the fundamental period of Equation (9). According to

standard HB theory, it is assumed that the steady-state solution of Equation (5) can be approximated using a finite-dimensional space $H = \mathrm{span}(X)$, where the set

$$X = \{\cos(p\omega t), \sin(p\omega t)\}_{p=1}^{N} \tag{10}$$

is complete. Then, the solution of Equation (5) can be approximated as $x(t) = \tilde{x}(t)$, with $\tilde{x}(t) \in H$ defined as a linear combination of the elements composing X as,

$$\tilde{x}_i(t) = \sum_{p=1}^{N} \alpha_i^p \cos(p\omega t) + \beta_i^p \sin(p\omega t), \tag{11}$$

with $i \in \mathbb{N}_n$. In order to describe Equation (11) in a compact form, let us define the auxiliary variables

$$\begin{aligned} \bar{X}_i &= [\alpha_i \beta_i ... \alpha_i^N \beta_i^N], \\ \Upsilon(t) &= [\cos(\omega t) \sin(\omega t) ... \cos(N\omega t) \sin(N\omega t)]^{\mathrm{T}}, \end{aligned} \tag{12}$$

with $\{\bar{X}_i, \Upsilon(t)\} \subset \mathbb{R}^N$. Thus, the approximation of the state vector of Equation (11) can be now written as

$$\tilde{x}(t) = \left[\bar{X}_1^{\mathrm{T}} ... \bar{X}_n^{\mathrm{T}}\right] \Upsilon(t). \tag{13}$$

In fact, the excitation force as introduced in Equation (9) can also be written now in terms of $\Upsilon(t)$ as

$$\tilde{x}(t) = [F_{\mathrm{ex}}\ 0]\Upsilon(t) = \bar{F}\Upsilon(t) \tag{14}$$

It is possible now to define the residual $R(\tilde{x}, f_{\mathrm{ex}}) = \dot{\tilde{x}} - f(\tilde{x}, f_{\mathrm{ex}})$ in terms of Υ as

$$R(\bar{X}, \bar{F}, \Upsilon) = \bar{X}\dot{\Upsilon} - f(\bar{X}\Upsilon, \bar{F}\Upsilon), \tag{15}$$

and a set of shifted generalised Dirac-delta functions as $D_c = \{\delta(t - t_j) = \delta_j\}_{j=1}^{q}$, with $q > nN$. Thus, the expansion coefficients $\bar{X}$ that approximate the solution of the state vector, as shown in Equation (13), can be computed using a Galerkin pseudo-spectral approach, which forces the projection of the residual function (15) to be 0. Note that this approximation is conducted for a broad-banded representation by considering the response of the system across the complete frequency spectrum.

4 CASE STUDY

The objective of the present study is the development of a HB framework that allows for the articulation of nonlinear effects in the analysis of WEC arrays. Therefore, the use of simple geometries as WECs is acceptable. Hence, the analysed WEC arrays are composed of identical heaving cylindrical bodies with a diameter (ϕ) of 10m, a draft of 10m, and a mass of $m = 7.9 \cdot 10^5$kg (assuming half of the cylinder is submerged). In total, the analysis is restricted to two different WEC array layouts: **L1** with two bodies in line and **L2** with three bodies in line, both parallel to the considered wave direction, as shown in Figure 1. In order to evaluate the impact of hydrodynamic interaction within the two WEC array configurations, several inter-device distances (d_{b}) are analysed, from 20m (2ϕ) to 2000m (200ϕ). Note that the PTO stiffness and damping employed in all cases are optimised for the isolated body case (a single WEC with no other devices in the area): $h_{\mathrm{pto}} = 2 \cdot 10^5$N/m and $k_{\mathrm{pto}} = -2 \cdot 10^5$Ns/m. Similarly, note that the viscous drag coefficient h_d is identical for all devices in the WEC array. Considering the high uncertainty in the definition of the viscous drag coefficient, and the fact that a precise estimate of this coefficient is beyond the scope of the present study, a standard value has been considered for the coefficient.

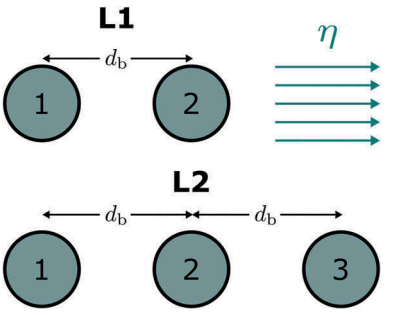

Figure 1. The two array layouts analysed.

5 RESULTS

The two WEC array configurations are analysed in order to (i) show the main benefits of the suggested HB approach and (ii) optimise the WEC array layout for each configuration, including nonlinear viscous effects. To that end, the new approach presented in this study must be adequately validated. Section (5.1) examines the suitability of the HB approach by comparing it against a traditional TD hydrodynamic model based on Cummins's equation, solved via direct convolution. A second-order numerical scheme (Runge-Kutta 2, RK) is used for the TD model, which is demonstrated to be adequate for both linear and nonlinear TD hydrodynamic models (Penalba and Ringwood 2019). On the other hand, Section (5.2) presents the results for different inter-device distances, identifying the optimal distance for both **L1** and **L2** configurations. For all the simulations analysed in this study, an irregular sea state is considered, with Figure 2

illustrating the JONSWAP-based theoretical spectrum, for which the significant wave height (H_s) is 2m and the peak period (T_p) 8s. In order to obtain results that are statistically consistent with the characteristics of this sea state, 25 different realisations are performed, and calculating the average motion and power absorption.

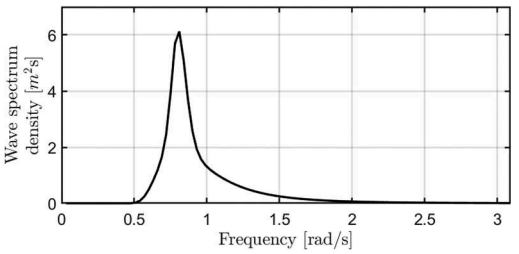

Figure 2. The theoretical JONSWAP-based wave spectrum for a $H_s = 2m$ and $T_p = 8s$ sea state.

5.1 *HB method validation*

The validation of the HB approach is first conducted with an isolated device, for which the results from the RK model and the HB approach are shown to be identical in Figure 3. The only difference arises at the beginning of the simulation (first 20s), where the RK model has not yet reached the steady-state solution.

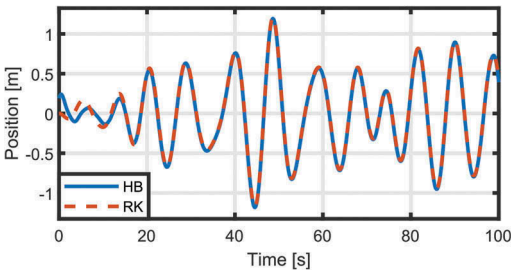

Figure 3. WEC position of an isolated body computed via the traditional TD model (RK) and the HB approach.

In addition to the isolated case, results for one of the WEC array configurations are also compared. The simplest configuration **L1** is selected, using the shortest inter-device distance ($d_b = 2\phi$), where the interaction should be strongest. Hence, the body motion of the two WECs in the array are compared, as illustrated in Figure 4, where the same conclusion as in the isolated case can be drawn: results from the TD and HB models are identical once the TD model reaches the steady-state solution. Therefore, one can confidently state that the HB approach is validated.

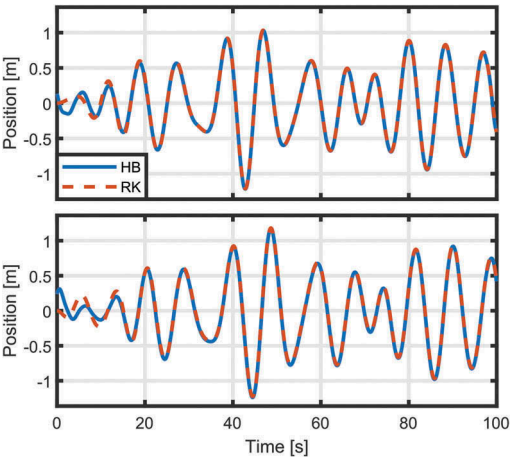

Figure 4. WEC position of an isolated body computed via the traditional TD model (RK) and the HB approachs (L1). inter-device distance = 20m.

Apart from the comparison in terms of body motion, the comparison of the computational burden of the different approaches is also interesting, since the HB approach is expected to be significantly more efficient. This comparison is carried out with respect to two main variables: (i) the simulation time and (ii) number of WECs in the array. Figure 5 illustrates the two comparison, top and bottom graphs illustrating the sensitivity of the approach to the simulation time and number of devices, respectively. Hence, one can see that the computational burden increases linearly for the TD simulation as the simulation length increases. In contrast, the computational burden increases exponentially in the case of the HB approach, meaning that the computational burden of the HB approach can even increase above the traditional RK model when the length of the simulation increases substantially. It should be noted that, for certain applications, relatively long simulations (between 15min up to 1h) are necessary, for which the current HB implementation would not be suitable. With the simulation time defined at 100s, as in Figures 3 and 4, the impact of increasing the number of devices in the WEC array is shown in the bottom graph in Figure 5. For the isolated device and small arrays (up to 3 devices) the computational burden of the HB approach is significantly lower. However, the ratio between the computational burden of the RK model and the HB approach reduces exponentially as the number of devices increases.

Therefore, one could say that the HB approach is not suitable for the simulation of WEC arrays with long simulations and a considerable number of devices. However, this statement should be clarified and the conclusion restricted to the present implementation of the HB approach. In fact, the literature shows that dividing the simulation into several

shorter parts, by means of relatively simple windowing techniques, can significantly reduce the computational burden (Wei et al. 2021), achieving computational burden ratios ($\Gamma = \frac{t_{sim_{RK}}}{t_{sim_{HB}}}$) between 10 and 20, as illustrated for simulations of up to 150s on the top graph in Figure 5. In fact, higher ratios could also be achieved by reducing the length of the windows, since the HB approach provides the steady-state results straightaway, avoiding the initial transient effect of traditional RK simulations.

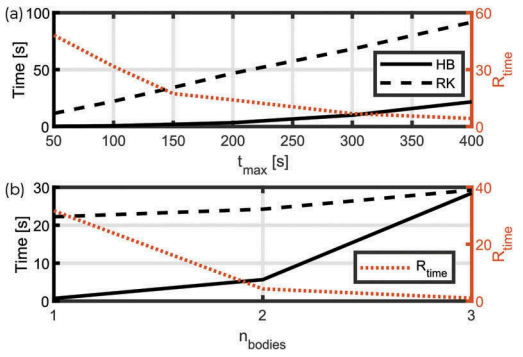

Figure 5. Comparison of the computational burden with respect to the length of the simulation (top) and number of devices in the WEC array (bottom). The red dotted-line represents the ratio between the time required by both methods ($R_{time} = t_{RK}/t_{HB}$).

5.2 *Layout optimisation*

Once the HB approach is validated, the WEC array layout can be assessed. Hence, power production for the two WEC array configurations, *i.e.* ***L1*** *and* ***L2***, is evaluated for different inter-device distances via the q-factor defined in Eq.(7). Figures 6 (a) and (b) show the q-factor for the **L1** and **L2** configurations, respectively, including linear and nonlinear HB models for both configurations.

In the case of the linear WEC array model, a strong fluctuation occurs within short inter-device distances ($d_b < 10$) for the **L1** configuration. Starting from highly destructive interaction ($q = 0.5$) at $d_b = 2\phi$, the interaction becomes constructive ($q = 1.5$ at $d_b = 5\phi$) and return to neutrality very quickly ($q = 1$ at $d_b = 7\phi$). Once this fluctuation stabilises, the interaction becomes positive again within a considerable range of inter-device distances ($10 < q < 45$). The q-factor evolution for the **L2** configuration is also very similar, with lower q-factor values at very short inter-device distances ($q = 0.2$ at $d_b = 2\phi$), and an intermediate constructive region that is slightly narrower and shifted to the left ($7 < q < 40$). After this intermediate region, the interaction becomes consistently destructive for both WEC array configurations, only reaching neutrality back again at the longest analysed inter-device distance ($d_b = 200\phi$). The same pattern of q-factor variation is also observed for different WEC array configurations in (Penalba et al. 2017), except for the destructive interaction region corresponding to long inter-device distances. One expects that the impact of the interaction disappears as the inter-device distance increases, as observed in (Penalba et al. 2017) and other similar studies.

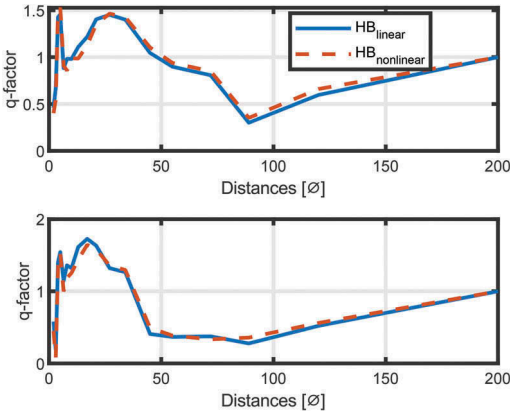

Figure 6. The evolution of the q-factor for different inter-device distances: (a) **L1** and (b) **L2** WEC array configurations. Blue continuous line denotes the linear model and the red dashed line the nonlinear viscous model.

This pattern appears to recur for the two WEC array configurations using a model with nonlinear viscous effects. Differences are almost imperceptible and focus on the intermediate region. Figure 7 shows a closer view of this intermediate region, where differences between the linear and nonlinear viscous models can be observed.

In the case of WEC array configuration **L1**, Figure 7 (a) shows that the nonlinear viscous force produces a shift in the q-factor, but no loss of absorbed power is identified. Hence, the intermediate region reaches the same q-factor level, but starts with longer inter-device distances ($d_b > 15$m) and extends further until $d_b = 50$m. In contrast, the impact of the nonlinear viscous effects for the **L2** WEC array configuration seems more related to a loss of power absorption capability. Figure 7 (b) illustrates that the intermediate region narrows slightly. Similarly to the **L1** configuration, the intermediate region starts about 5ϕ later than for the linear case, but ends at the same point. In addition, the peak factor is reduced by about 5% due to viscous effects. This attenuation is a typical effect of the viscous effects that is widely covered in the literature.

Therefore, in both WEC array configurations, the optimal inter-device distance should be selected within the intermediate range, ensuring constructive interaction. However, note that a single sea state is used in this study. For precise layout optimisation, the

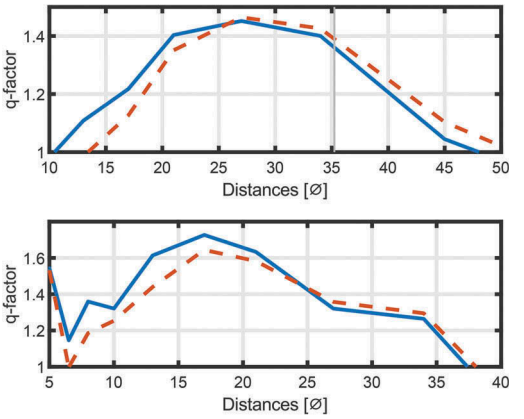

Figure 7. The evolution of the q-factor in the intermediate region: (a) **L1** and (b) **L2** WEC array configurations.

behaviour of the WEC array, and its power absorption capability, should be assessed for the entire operational region, considering all the relevant sea states of the specific location, as in (Penalba et al. 2017).

6 CONCLUSIONS AND FUTURE WORK

The present paper presents a novel mathematical model for the evaluation of wave energy converter array layout assessment based on the Harmonic Balance approach. This approach combines frequency and time-domain interpretations and enables a computationally efficient articulation of nonlinear and non-ideal effects. In this study, only nonlinear viscous effects are included for a preliminary implementation of the approach, and two relatively simple wave energy converter array configurations (**L1** and **L2**) are studied, comprising two and three devices, respectively.

The HB approach is first validated against a traditional nonlinear time-domain model based on the Cummins' equation solved via direct convolution and a second-order Runge-Kutta numerical scheme. Validation is carried out for an isolated device and the two array configurations resulting in the following main conclusions:

- Results from both approaches are identical for the steady-state solution. The HB approach directly provides the steady-state results, while the traditional time-domain model includes an initial transient period.
- The computational burden of the present implementation of the HB approach varies exponentially with the simulation length and number of devices included in the array, while a linear increase is observed in the case of the traditional time-domain simulation.

However, the computational burden of the present implementation of the HB approach can be improved significantly by modifying the implementation of the approach dividing the simulation into several windows. Note that the HB approach is particularly computationally efficient for short simulation times. Therefore, using an efficient windowing technique, the HB approach can be considerably more efficient than the traditional time-domain method. In fact, this advantage in computational cost is especially relevant when more complex nonlinear effects, such as nonlinear Froude-Krylov forces or nonlinear power take-off dynamics, are included.

Finally, the impact of the nonlinear viscous effects on the optimal layout is shown to be relatively low. In the two-device **L1** array configuration, the nonlinear viscous effects insert a shift in the q-factor, shifting the constructive intermediate region to longer inter-device distances. In contrast, viscous effects in the three-device **L2** array configuration insert an attenuation of the power absorption capabilities of the array, reducing the peak q-factor. However, the inter-device distance at which this peak appears does not vary.

Based on the results obtained in this study, future research lines include:

- The extension of the analysis to consider the entire wave climate of a specific location including all the relevant sea states;
- The implementation of a windowing technique to reduce the effective simulation length of each window and reduce the computational cost;
- The articulation of other hydrodynamic nonlinear effects, such as nonlinear Froude-Krylov forces;
- The implementation of a more sophisticated power take-off system with nonlinear and non-ideal effects; and
- The implementation of advanced control structures that enable the power maximisation of the wave energy converters in the array.

Incorporating all these aspects into the array model is crucial for precise array layout optimisation. In this sense, the HB approach presented in this study enables implementation of all these aspects in a computationally efficient manner, which is vital for optimisation purposes.

ACKNOWLEDGEMENTS

NThis material is based upon works supported by the research project PID2021-124245OA-I00 funded by MCIN/AEI/10.13039/501100011033 and by ERDF A way of making Europe, and the project KK-2022/00090 funded by the Basque Government's ELKARTEK research program. The authors would also like to acknowledge funding by Science Foundation Ireland through the *Research Centre for Energy, Climate and Marine (MaREI)* under Grant 12/RC/2302_P2. This project has received funding from the European Union's Horizon 2020 research and innovation program under the Maire Sklodowska - Curie grant agreement No. 101034297.

REFERENCES

Babarit, A. (2010). Impact of long separating distances on the energy production of two interacting wave energy converters. *Ocean Engineering 37*(8), 718–729.

Borgarino, B., A. Babarit, & P. Ferrant (2012). Impact of wave interactions effects on energy absorption in large arrays of wave energy converters. *Ocean Engineering 41*, 79–88.

Cummins, W. E. (1962). The impulse response function and ship motions. *Schiffstechnik 47*, 101–109.

Gaebele, D. T., M. E. Magaña, T. K. Brekken, & O. Sawodny (2020). State space model of an array of oscillating water column wave energy converters with inter-body hydrodynamic coupling. *Ocean Engineering* 195.

Garcia-Rosa, P. B., G. Bacelli, & J. V. Ringwood (2015). Control-informed optimal array layout for wave farms. *IEEE Transactions on Sustainable Energy 6*(2), 575–582.

Giorgi, G. & N. Faedo (2022). Performance enhancement of a vibration energy harvester via harmonic time-varying damping: A pseudospectral-based approach. *Mechanical Systems and Signal Processing 165*, 108331.

Krack, M. & J. Gross (2019). *Harmonic balance for nonlinear vibration problems*, Volume 1. Springer.

Magana, M. E., C. Parlapanis, D. T. Gaebele, & O. Sawodny (2021). Maximization of Wave Energy Conversion into Electricity Using Oscillating Water Columns and Nonlinear Model Predictive Control. *IEEE Transactions on Sustainable Energy 13*(3), 1283–1292.

Mérigaud, A. & J. V. Ringwood (2017). A nonlinear frequency-domain approach for numerical simulation of wave energy converters. *IEEE Transactions on Sustainable Energy 9*(1), 86–94.

Morison, J., J. Johnson, & S. Schaaf (1950). The force exerted by surface waves on piles. *Journal of Petroleum Technology 2*(05), 149–154.

Ogilvie, T. F. (1964). Recent progress toward the understanding and prediction of ship motions. In *5th Symposium on naval hydrodynamics*, Volume 1, pp. 2–5. Bergen, Norway.

Penalba, M. & J. V. Ringwood (2019). A high-fidelity wave-to-wire model for wave energy converters. *Renewable Energy 134*, 367–378.

Penalba, M., I. Touzón, J. Lopez-Mendia, & V. Nava (2017). A numerical study on the hydrodynamic impact of device slenderness and array size in wave energy farms in realistic wave climates. *Ocean Engineering 142*, 224–232.

Penalba, M., A. Ulazia, J. Saénz, & J. V. Ringwood (2020). Impact of Long-term Resource Variations on Wave Energy Farms: The Icelandic case. *Energy 192*, 116609.

Wei, Y., A. Bechlenberg, M. van Rooij, B. Jayawardhana, & A. I. Vakis (2021). Modelling of a wave energy converter array with a nonlinear power take-off system in the frequency domain. *IET Renewable Power Generation 15*, 3220–3231.